Micron 116 (2019) 108–115

Contents lists available at ScienceDirect

Micron

journal homepage: www.elsevier.com/locate/micron

Finite element modeling of living cells for AFM indentation-based biomechanical characterization

Yi Liu, Keyvan Mollaeian, Juan Ren*

Department of Mechanical Engineering, Iowa State University, Ames, IA 50011, USA

ARTICLE INFO

Keywords:
Cell mechanotransduction
AFM
FEM
Contact mechanics

ABSTRACT

Mechanotransduction—the process living cells sense and respond to forces—is essential for maintenance of normal cell, tissue, and organ functioning. To promote the knowledge of mechanotransduction, atomic force microscope (AFM) force-indentation has been broadly used to quantify the mechanical properties of living cells. However, most studies treated the cells as a homogeneous elastic or viscoelastic material, which is far from the real structure of cells, and the quantified mechanical properties cannot be used to investigate the inner working mechanism of mechanotransduction, such as internal force distribution/transduction. Therefore, a new viscoelastic finite element method (FEM) model is proposed in this study to simulate the force response of living cells during AFM force-indentation measurement by accounting for both the cell elasticity and viscoelasticity. The cell is modeled as a multi-layered structure with different mechanical characteristics of each layer to account for the depth-dependent mechanical behavior of living cells. This FEM model was validated by comparing the simulated force-indentation curves with the AFM experimental data on living NIH/3T3 cells, and the simulation error was less than 10% with respect to the experiment results. Therefore, the proposed FEM model can accurately simulate the force response of living cells and has a potential to be utilized to study and predict the intracellular force transduction and distribution.

1. Introduction

Mechanotransduction—the continual process of sensing, transmission, and response to external mechanical stimuli of live cells—is essential for maintenance of normal cell, tissue, and organ functioning, such as proliferation, differentiation and tissue organization (Wozniak and Chen, 2009; Mathieu and Loboa, 2012; Abu-Lail et al., 2006; Amano et al., 1996; Liu, 2006; Moeendarbary and Harris, 2014). Understanding the basic working mechanism of mechanotransduction can lead to breakthrough improvements in biochemical and biomedical sciences and engineering. For example, it is suggested that the cure of cardiac hypertrophy and heart failure leans on a comprehensive understanding of cardiovascular muscle mechanotransductive process (Stansfield et al., 2014; Lyon et al., 2015), and proper mechanical stimuli can help to boost the mammalian adaptive immune system by regulation of T-cell functions (Chen and Zhu, 2013; Previtera, 2014). To understand the mechanical properties of cells and understand the intracellular force transduction process, atomic force microscope (AFM) indentation has been broadly used for living cell mechanical characterization due to its superior capability of the precise force and location control (Giridharagopal et al., 2012) compare to other experimental techniques, such as optical/magnetic tweezers (Gosse and Croquette, 2002; Honarmandi et al., 2011; Polacheck et al., 2014), and micropipette aspiration (Liu and Shao, 2014; Evans et al., 2005). However, AFM indentation measurement, like all other experimental approaches, can only quantify the cell deformation under various mechanical stimuli (Yan et al., 2017; Efremov et al., 2017)—the inner working mechanisms by which living cell senses and responses to applied mechanical excitation still remains unclear.

To promote the understanding of the force transduction process in living cells, finite-element method (FEM) has been implemented to simulate the internal stress distribution and transduction in response to the external mechanical stimuli. By defining the geometry and material properties of the cell, the internal cellular force transduction can be readily simulated subject to the given boundary conditions and excitation profile. Baaijiens et al. created a 2D non-structural model of a chondrocyte with homogenous elasticity to predict the cell's response subjected to the micropipette aspiration (Baaijens et al., 2005). Caille et al. developed a 2D structural model of an endothelial cell with homogeneous incompressible hyperelasticity to achieve the mechanical properties subjected to compression (Caille et al., 2002). Chen et al. developed a 2D model for AFM nanoindentation on chondrocyte by

* Corresponding author.
E-mail address: juanren@iastate.edu (J. Ren).

https://doi.org/10.1016/j.micron.2018.10.004
Received 28 June 2018; Received in revised form 11 October 2018; Accepted 11 October 2018
Available online 14 October 2018
0968-4328/

treating the cells as a homogeneous viscoelastic material (Chen and Lu, 2012). Although the 2D models can help to simulate intracellular force analysis to some extent, they cannot be applied to study the force distribution and/or transduction along the vertical direction, which is very crucial for nanoindentation case studies. Therefore, Bursa et al. extended the 2D model to the nonstructural 3D model based on a smooth muscle cell with homogeneous elasticity, in order to obtain the material parameters by Mooney-Rivlin hyperelastic strain energy density function (Bursa and Fuis, 2009). McGarry and Prendergast developed six idealized-shaped structural models, described as increasingly spreading shapes, of chick embryo fibroblasts adherent to substrate, for the purpose of verifying the availability of these models in evaluating the cellular structural response to different compression, indentation, and magnetic tweezers tests (McGarry and Prendergast, 2004). However, none of these models have considered both the elastic and viscoelastic behavior of cells at the same time nor have been validated with experimental results. Furthermore, the assumption of homogeneity and use of idealized geometry in the 3D models are inconsistent with the true properties of living cells—the heterogeneous multi-layered nature. Without modeling the cell close to its true structure, it is nearly impossible to understand the force transduction process among different cell structures. Therefore, a more realistic FEM model which considers the actual shape and structure, as well as elastic and viscoelastic properties of living cells, needs to be developed and be further validated with experimental results to improve the understanding of mechanotransduction process.

In this study, a FEM model is proposed to simulate the force response of living cells during AFM indentation. The FEM cell model consists a multi-layered structure, and its geometric size and material properties were determined by cell image and indentation experiments conducted by AFM, respectively. The proposed FEM model was validated by comparing the simulated force-indentation curves with the AFM experimental data, and the simulation error was less than 10% with respect to the experiment results. Therefore, the proposed model provides a way of promoting an in-depth understanding of mechanotransduction.

2. Methods

2.1. Cell preparation

Primary mouse embryonic fibroblast cells (NIH/3T3) were seeded in 35mm tissue culture dish (Corning, NY, USA), and cultured in Dulbecco's Modified Eagle's Medium (ATCC, Rockville, MD, USA) with 10% (V/V) calf bovine serum (Sigma-Aldrich, ST. Louis, MO, USA) and 1% (V/V) penicillin-streptomycin (Gibco, Grand Island, NY, USA). Immediately after seeding, the cells were kept at 37 °C in a 5% CO_2 incubator for 24 h. Then the dish was rinsed with the aforementioned cell culture medium (warmed up to 37 °C) to remove dead and loosely attached cells right before the AFM measurement. The cell viability was guaranteed both before and during testing since only cells with normal morphology (i.e., with cell membrane smoothly spread out on the substrate (Clynes, 2012; Paul et al., 1970)) observed under the microscope were measured during the experiment, and the AFM measurement data were smooth without any sudden variations.

2.2. Atomic force microscope

AFM measurements were performed at room temperature on a state-of-the-art biomechanical characterization system (BioScope Resolve, Bruker Inc., CA, USA) which is integrated with an inverted optical microscope (IX73, Olympus, Japan). The drive voltage, the piezo displacement data, and the cantilever deflection of the AFM were acquired using an NI PCIe-6353 DAQ board (National Instrument, TX, USA) with Matlab Simulink Desktop Real-Time system (Mathworks, MA, USA).

NIH/3T3 cells were probed in the aforementioned medium using a colloidal probe cantilever (Novascan, IA, USA) with a sphere radius of 2.5 μm and cantilever spring constant of 0.03 N/m (calibrated using thermal tune approach (Hutter and Bechhoefer, 1993)). Before and after the measurements, the relationship between the photodiode signal and the cantilever deflection (the deflection sensitivity, S) was calibrated using force curves at a bare region of a silicon sample. Therefore, the AFM probe-sample interaction force, $F(t)$, was quantified as,

$$F(t) = k \times S \times d(t), \tag{1}$$

where k is the cantilever spring constant, and $d(t)$ is the cantilever deflection increase since contact is first established between the probe and the cell. The indentation depth, $\delta(t)$ was then quantified as,

$$\delta(t) = z(t) - d(t) \tag{2}$$

where $z(t)$ is the height of the probe (i.e., the AFM piezo displacement) with respect to its position at the initial probe-sample contact.

2.3. Finite element model

The process by which the AFM probe indented into the cell membrane and underlying cytoskeleton was modeled. A 3D finite element method (FEM) model was created using ANSYS 17.2. In this paper, the measurements were presented as mean ± S.D.

2.3.1. Cell image and FEM design

The AFM probe (i.e., the bead indenter) was modeled as a rigid sphere with the radius of 2.5 μm as its real shape. The FEM cell model consists of three layers: the semi-ellipsoid outer layer represents the cell membrane and underlying cytoplasm; the middle layer represents the cell nucleus which has a similar spreading shape as the cytoplasm with a distance of 0.1 μm from the substrate; the inner layer ellipsoid represents the cell nucleus, which is the hardest part of a cell. The FEM model of the probe-cell contact system is illustratively shown in Fig. 1.

Ten different NIH/3T3 cells seeded in cell culture dishes were imaged using contact mode AFM in the aforementioned cell culture medium at room temperature to determine the geometric size of the cell for the proposed FEM model. The AFM topography image allowed us to directly quantify the 3D size of NIH/3T3 cells. As an example shown in Fig. 2, the shape of NIH/3T3 cells attached to the cell culture dish could be approximated as a semi-ellipsoid. The ten imaged cells had a length of 60.1 ± 4.2 μm, a width of 13.2 ± 2.7 μm, and a height of 6.3 ± 1.5 μm, respectively. The nucleus had a length of 11.3 ± 2.1 μm, and a width of 10.5 ± 1.3 μm. The size of the nucleolus was estimated as 2.3 ± 0.9 μm in length, and 1.7 ± 0.6 μm in width based on captured optical images of the cells (see Fig. 2 for an example of one cell).

Therefore, according to AFM and optical images, the cell in the FEM model was approximated as a semi-ellipsoid with the height of 6 μm, the major axis of 30 μm, and the minor axis of 6 μm. The second layer (the nucleus) of the FEM was modeled as a semi-ellipsoid with the height of 5.4 μm, the major axis of 6 μm, the minor axis of 5.4 μm, and the distance of 0.1 μm from the substrate. The inner layer (nucleolus) was an ellipsoid with the major axis of 3 μm, and the minor axis of 2 μm.

2.3.2. Material properties

The cell model and the indenter were treated as an isotropic elastic-viscoelastic body and an isotropic elastic body, respectively. Specifically, the cell is treated as an elastic body along the normal direction, and as a viscoelastic body (e.g., generalized Maxwell solids) along the shear direction. As the AFM sphere indenter was made of SiO_2, it was thus treated as a linear elastic and isotropic continuum with the Young's modulus of 70 GPa, and the Poisson's ratio of 0.24 (Yeganeh-Haeri et al., 1992). For simplicity, the Poisson's ratio of the cell was chosen as 0.37 for all the three layers as used previously (Bursa and Fuis, 2009; Shin and Athanasiou, 1999). As shown in previous

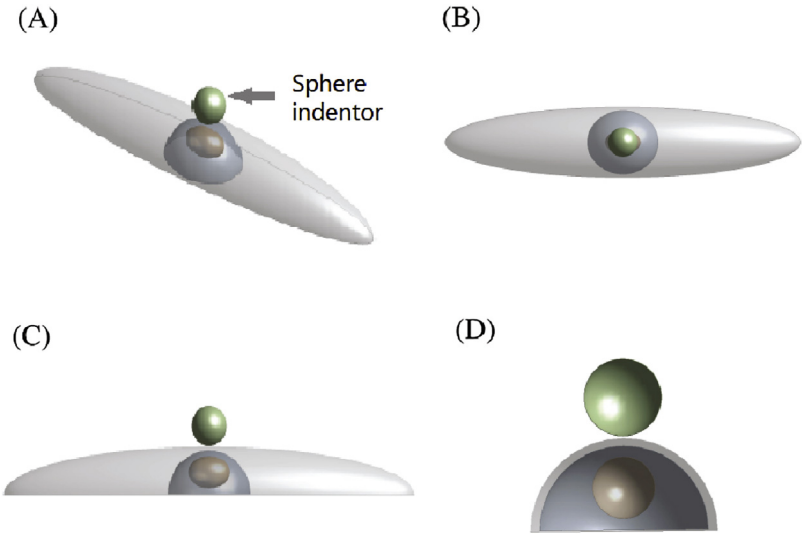

Fig. 1. (A) The finite element model designed in ANSYS; (B), (C), and (D) are the top view, the major-axis view, and the minor-axis view of the FEM model, respectively.

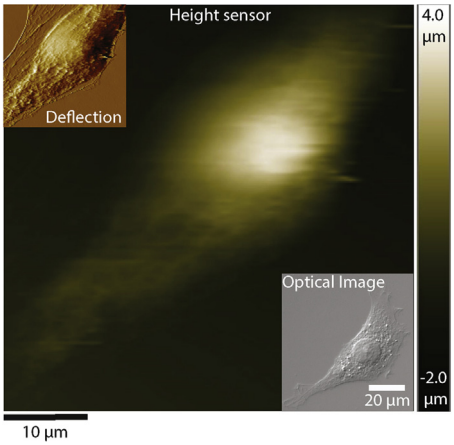

Fig. 2. An example of AFM topography image of a NIH/3T3 cell seeded on a cell culture dish.

studies that living cell elasticity is depth-dependent (Sedef et al., 2006; Chung and Mansour, 2014), the cell model was assumed to have different Young's modulus at each layer, which were determined using an elastic contact model (e.g., the Hertz model) and the data from AFM force-curve measurement measured at a low indenting velocity (i.e., the elastic behavior of the cells is dominant) (Liu, 2006; Moeendarbary and Harris, 2014). The viscous property of the cell was quantified by fitting the force-relaxation measurement results using the Prony series model. The details of how to quantify the cell material properties are presented below.

(i) *Quantification of the Young's modulus—elastic model.* To quantify the Young's modulus, living cells are conventionally treated as an isotropic elastic body, such as in the Sneddon model or the Hertzian model, depends on the indenter shape (Bursa and Fuis, 2009). As the Young's modulus of the spherical indenter is at least three orders higher than that of living cells (70 GPa vs. a couple of kPa), also, the strain level was less than 20% in the cell, the Young's modulus of NIH/3T3 cells can be readily quantified using the thin-layer Hertz model at a low indenting velocity as (Faria et al., 2008; Chen, 2014):

$$F(t) = \frac{4E\sqrt{r}}{3(1-\nu^2)}\delta(t)^{\frac{3}{2}} f_1(X) \tag{3}$$

where $r = 2.5\,\mu m$ is the equivalent radius of the spherical bead, $\nu = 0.37$ is the Poisson's ratio of the cell. $f_1(X)$ is the geometrical correction factor which is given by,

$$\begin{aligned} f_1(X) = & \left[1 - \frac{2\alpha_0}{\pi}X + \frac{4\alpha_0^2}{\pi^2}X^2\right. \\ & - \frac{4\alpha_0^2}{\pi^2}\left(\alpha_0^3 + \frac{4\pi^2}{15}\beta_0\right)X^3 \\ & \left. + \frac{16\alpha_0}{\pi^4}\left(\alpha_0^3 + \frac{3\pi^2}{5}\beta_0\right)X^4\right] \end{aligned} \tag{4}$$

and,

$$X = \frac{\sqrt{r\delta(t)}}{h} \tag{5}$$

where h is the cell height,

$$\alpha_0 = -\frac{1.2867 - 1.4678\nu + 1.3442\nu^2}{1-\nu} \tag{6}$$

and,

$$\beta_0 = \frac{0.6387 - 1.0277\nu + 1.5164\nu^2}{1-\nu} \tag{7}$$

Consider the depth-dependent elasticity of living cells (Liu, 2006; Moeendarbary and Harris, 2014), we propose to quantify the Young's modulus of the cytoplasm and nucleus separately. Based on the shape of the sphere indenter, we assumed that the probe-sample contact area was semispherical given the indentation depth used in this study did not exceed the radius of the indenter. Since the distance between the nucleus and the substrate was negligible compared to the height of the cell, so was the thickness of the cell membrane, it is reasonable to consider the cell as a three-layered structure during the AFM indentation process: the membrane + cytoplasm layer (or cytoplasm layer), the nucleus layer, and the nucleolus layer as showing in Fig. 3.

To quantify the Young's modulus of these three layers, the NIH/3T3 cells were indented at a very slow speed (0.08 μm/s) with an indentation depth much larger than the thickness of cytoplasm. So that during the indenting process, the stress of the cell within the probe-sample contact region was uniformly distributed and the cell was at steady state (Mijailovich et al., 2010). The third layer (nucleolus) is a very dense fibrillar component inside the nucleus, and its size is much smaller than the cell height and the thickness of the cytoplasm (Shaw and Brown, 2012). Compare the size and stiffness of the third layer with the first and second layers, the deformation of the nucleolus caused by AFM indentation is treated as negligible (Shaw and Brown, 2012). Therefore, the uniform distribution of intracellular stress yields,

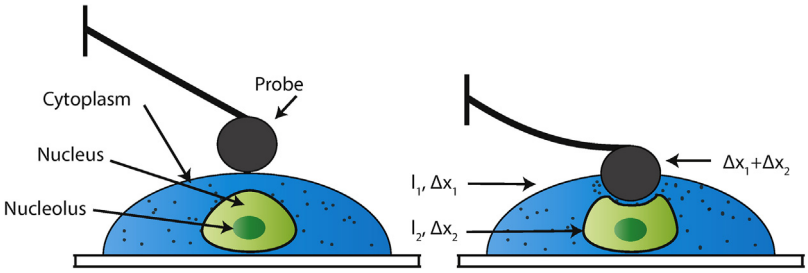

Fig. 3. Schematic of the simplified finite element model for AFM indentation measurement on the top the nucleus of the living cell with a spherical indenter.

$$\frac{F}{A} = E_c\frac{\Delta x_1}{l_1} = E_n\frac{\Delta x_2}{l_2} = E_{c-n}\frac{\Delta x_1 + \Delta x_2}{l_1 + l_2} \tag{8}$$

where $\frac{F}{A}$ is the stress uniformly distributed within the probe-sample contact region, E_c is the Young's modulus of cytoplasm, E_n is the Young's modulus of the nucleus, and E_{c-n} is the combined Young's modulus of cytoplasm and nucleus. Δx_1 and Δx_2, l_1 and l_2 are the displacement and thickness of cytoplasm and nucleus, respectively, as showing in Fig. 3. The thicknesses of l_1 and l_2 were specified according to the geometrical size of the designed model, and the displacements were quantified based on the AFM force-curve measurement. The Young's modulus of cytoplasm (E_c), and the combined Young's modulus (E_{c-n}) were obtained from the AFM force-curve experiments at small and large indentation depths, respectively. Specifically, E_c was determined using the measured force and indentation when the indentation was small enough so that the deformation of the nucleus is negligible (i.e., $\Delta x_2 = 0$ and $\delta = \Delta x_1$), then when the indentation was big enough to deform both the cytoplasm layer and the nucleus, E_{c-n} could be quantified since $\delta = \Delta x_1 + \Delta x_2$. Note that the contact area A could be quantified readily using δ as the indenter was an ideal sphere. Then the Young's modulus of the nucleus (E_n) was quantified using Eq. (8).

(ii) *Quantification of relative moduli and relaxation time—Viscoelastic model.* To describe the viscoelastic behavior of NIH/3T3 cell—the dynamic nature of living cells, a linear viscoelastic model, i.e., the Prony series model, was adopted (Sedef et al., 2006; Chung and Mansour, 2014).

Specifically, the living cells are treated as the generalized Maxwell solids, which consists of Newtonian dashpots and Hookean springs (Del Nobile et al., 2007; Kaliske and Rothert, 1997). Therefore, the shear modulus, $G(t)$, can be quantified from the force-relaxation measurement, i.e., the AFM probe rests on the cell after indentation (Sedef et al., 2006), as

$$G(t) = \frac{3F_{vs}(t)(1-\nu)}{8\delta_{vs}\sqrt{r\delta_{vs}}f_1(X_{vs})} \tag{9}$$

where $F_{vs}(t)$ is the probe-cell interaction force during the relaxation process, δ_{vs} was the cell indentation at the beginning of the relaxation process. $f_1(X_{vs})$ is the geometrical correction factor which is given by,

$$\begin{aligned} f_1(X_{vs}) = {} & [1 - \tfrac{2\alpha_0}{\pi}X_{vs} + \tfrac{4\alpha_0^2}{\pi^2}X_{vs}^2 \\ & - \tfrac{4\alpha_0^2}{\pi^2}(\alpha_0^3 + \tfrac{4\pi^2}{15}\beta_0)X_{vs}^3 \\ & + \tfrac{16\alpha_0}{\pi^4}(\alpha_0^3 + \tfrac{3\pi^2}{5}\beta_0)X_{vs}^4] \end{aligned} \tag{10}$$

and,

$$X_{vs} = \frac{\sqrt{r\delta_{vs}}}{h} \tag{11}$$

where α_0 and β_0 are given as Eqs. (6) and (7), respectively. According to the generalized Maxwell model, the relaxation modulus can be further expanded using the Prony series (Chung and Mansour, 2014), as

$$G(t) = G_0[\alpha_\infty + \sum_{j=1}^{N}\alpha_j e^{\frac{-t}{\tau_j}}] \tag{12}$$

where G_0 is the instantaneous modulus, i.e, $G_0 = G(t)|t \to 0$. α_∞ is the normalized infinite modulus, α_j is a material related relative moduli constant, and τ_j is the material relaxation time constant. In this study, we considered the one-term Prony series bellow, i.e., $N = 1$, which has been proven fit the force-relaxation data of living cells fairly well (Chung and Mansour, 2014; Darling et al., 2006).

$$G(t) = G_0[\alpha_\infty + \alpha_1 e^{\frac{-t}{\tau_1}}] \tag{13}$$

G_0, the instantaneous shear modulus, was obtained at the beginning of the force relaxation curves (i.e., $G(0) = G_0$ at $t = 0$). Therefore, according to Eq. (13), $\alpha_\infty + \alpha_1 = 1$. Then, the viscoelastic parameters of NIH/3T3 cell, α_∞, α_1, and τ_1, were obtained by fitting the relaxation modulus quantified from Eq. (9) using Eq. (13).

2.3.3. FEM conditions

Since the substrate (cell culture dish) was much harder than the cells, the basal surface of the cell was constrained to zero displacement. We also assumed that no relative displacement existed between the layers inside of the cell (no-slip condition). The probe-cell interaction force was limited to repulsive tension only (no tractions forces), and stable-probe sample contact was assumed throughout the force measurement process (McGarry and Prendergast, 2004), i.e., the apical surface of the cell (membrane) was in complete contact with the AFM tip. The cell surface that was not in direct contact with the probe was prescribed to zero stress and the side edges of the domain were free to move.

The connections of different material layers were set as bonded, and the default triangle elements were used to discretize the cell membrane and underlying cytoskeleton (the first layer). The shape checking method of the generated elements was set to be aggressive mechanical. Elements of 0.8 μm were used for the spherical tip model and 0.4 μm was the maximum for the three-layered cell model. The mesh was chosen by systematically reducing its size until the results were independent of element size.

3. Results

3.1. Young's modulus

To quantify the cell elasticity, NIH/3T3 cells were indented at the velocity of 0.08 μm/s with a targeted indentation depth of 1 μm. This operation was repeated five times (each time on a different cell), and the obtained force-indentation curves are shown in Fig. 4. The reason of choosing such a slow indentation velocity is to ensure that the intracellular stress was uniformly distributed and the elastic behavior dominated the cellular mechanical response during the indenting process—to satisfy the condition of the Hertz model and the assumption of Eq. (8), respectively. Then each force-indentation curve was fitted using the corrected Hertz contact model (Eq. (3)) to quantify the Young's modulus. To be consistent with the FEM model, the force-indentation curve was divided into two segments to quantify the Young's modulus of the cytoplasm E_c and the cytoplasm-nucleus combined Young's modulus E_{c-n}. The separation point of the curve segments was

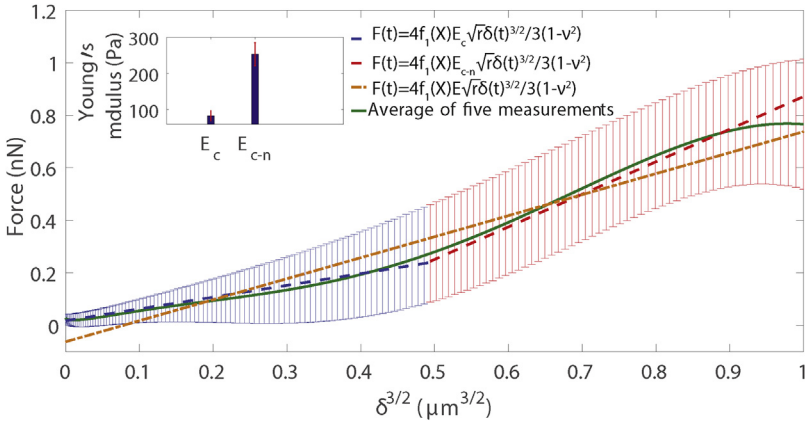

Fig. 4. The error bars represent the AFM force-indentation curve range for all the five measurements (for the indentation depth of 1 μm). Each force-indentation$^{3/2}$ curve was divided into two parts to quantify E_c and E_{c-n}. The intersection point ($\delta \approx$ 0.625 μm) of the curve segments was determined to achieve the best fitting results using the corrected Hertz contact model (with an RMS fitting error of 0.56 % ~4.97% for the five measured curves). The blue part is used to obtain E_c = 83.77 ± 14 Pa for the cytoplasm layer, and E_{c-n} = 253.7 ± 31.8 Pa was quantified through curve fitting the red segment. For comparison, the average curve of the AFM measurement (in green) was also fitted as a whole using the corrected Hertz contact model (in orange), which led to an RMS fitting error of 16.79%.

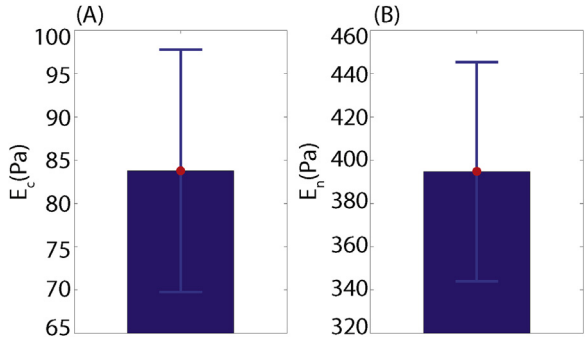

Fig. 5. The quantified Young's modulus: (A) of the cytoplasm layer E_c = 83.77 ± 14 Pa, (B) of the nucleus E_n = 395 ± 50.67 Pa. n = 5.

determined to achieve the best fitting results with an RMS fitting error (0.56 % ~4.97% for the five measurements) of Hertz contact model for the entire curve. Based on the height of the cell and nucleus size chosen in the FEM, E_c = 83.77 ± 14 Pa and E_{c-n} = 253.7 ± 31.8 Pa was quantified (see Fig. 4). Then E_n = 395 ± 50.67 Pa (nucleus) was quantified using Eq. (8). The quantified Young's moduli are shown in Fig. 5. These quantified Young's moduli match the results from previous studies on AFM micro-indentation of NIH/3T3 cells fairly well (Nawaz et al., 2012; Guilak and Mow, 2000; Guilak et al., 2000). Specifically, as reported by Kamm et al. (2000) and Nawaz et al. (2012) (Nawaz et al., 2012; Guilak et al., 2000), the Young's modulus of cytoplasm was about 100 Pa, and the Young's modulus of the nucleus was about 400 Pa. So the Young's modulus values in our experiments concur with the previous sources. Furthermore, fitting the average force indentation curve (the average of the five measurements) as a whole led to an RMS fitting error of 16.79%, which demonstrated that for the chosen targeted indentation, the cells should be treated as a heterogeneous material when estimating the Young's modulus.

As the measured Young's moduli were validated by previous results, the mean values of E_c and E_n were adopted as the Young's modulus of the first and second layers of the proposed FEM model, respectively. Since it's very challenging to quantify the elasticity of the nucleolus, the upper range of E_n–450 Pa was used as that of the inner layer in the FEM model. Actually, given the size of the nucleolus is about 10% of the nucleus, it is expected that the Young's modulus of the inner layer would not affect the FEM model analysis much.

3.2. Relative moduli and relaxation time

To quantify the cell viscoelasticity, NIH/3T3 cells were indented at the same velocity of 0.08 μm/s until the indentation depth of 1 μm was reached, and the bead indenter was held at the corresponding position for 11 seconds to get the force-relaxation curve (see Fig. 6). This operation was repeated five times (each time on a different cell). In order to get the cell viscoelastic parameters, the shear modulus curve was obtained using Eq. (9), and then fitted with the one-term Prony series (N = 1 in Eq. (12)). According to the relaxation curves, we quantified that G_0 = 145 ± 20.555 Pa. This yielded a fitting result of α_1 = 0.6108 ± 0.095 (relative moduli) and τ_1 = 5.56 ± 0.07 s (relaxation time) (see Fig. 7). The mean values of α_1 and τ_1 were adopted as the relative moduli and relaxation time, respectively, for all layers of the cell in the FEM.

3.3. Finite element modeling results

To validate the proposed FEM, the force-indentation curves generated from FEM simulation were compared to those obtained from the AFM indentation experiments under the same measurement conditions.

For the better demonstration of the validity of the proposed FEM, the indenting velocities and indentation depths used for validation were intentionally chosen differently from those used for the cell mechanical property quantification. For FEM simulation, the probe-cell contact interface was set to deform at a velocity of 0.1 μm/s until three displacements were reached: 0.7 μm, 1 μm, and 1.2 μm. When the contact interface displacement (i.e., cell indentation) was specified in the FEM, the model computed the probe-cell interaction force based on the specified probe and cell material properties, accordingly. The FEM simulation results at the targeted indentations are shown in Fig. 8. The AFM indentation measurements were performed using the same indenting velocity and targeted indentation depths, and for each depth, the measurement was repeated five times with each time on a different cell. The FEM force-indentation curves were shown and compared to the average AFM measurements under each condition in Fig. 9. The FEM force vs. indentation curves match the AFM indentation measurement results well. Specifically, the entire force-indentation curves of the FEM were close to the experiment results under similar indenting conditions: the RMS relative difference of the entire force-indention curve between the FEM result and the AFM indentation data was 6.67% (with respect to the AFM measurement result) at the indentation of 0.7 μm, the FEM force-indentation curve at the targeted indentation of 1.0 μm was 8.46% different with respect to the AFM measurement at the same indentation depth, and the RMS difference between the FEM force-indentation curve and the AFM indentation experiment data was 9.72% different (with respect to the AFM measurement) for the indentation of 1.2 μm. Consider the material property measurement uncertainty, the FEM simulation results match the AFM experiment results fairly well.

In the aforementioned research, the Poisson's ratio was assumed as 0.37. Theoretically, the value of Poisson's ratio could affect the simulation result. According to the previous studies, the reported Poisson's ratios of living cells are mostly between 0.35 and 0.45 (Trickey et al., 2006). Therefore, to verify the effect of different Poisson's ratio values

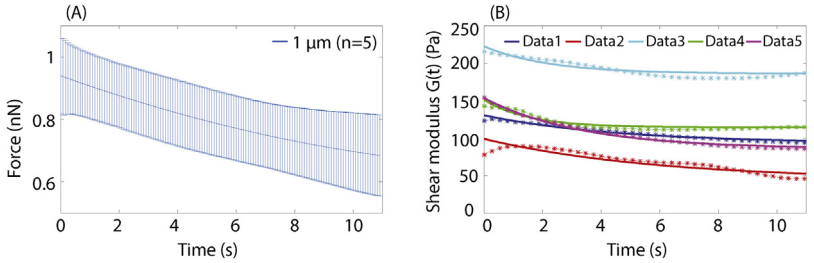

Fig. 6. (A) The AFM force-relaxation curves when the initial indentation depth was 1 μm. The blue bars denote the force data range of the five measurements. (B) The shear modulus curve obtained using (A) and Eq. (12) (the star curves) of the five force-relaxation measurements, and their Prony series fitting results (solid lines).

on the proposed model, five Poisson's ratios (e.g., 0.35, 0.37, 0.39, 0.41, 0.45) were applied to the material parameter of the model. The probe-cell contact interface was set to deform at a velocity of 0.1 μm/s until the displacement was reached. As an example, for the targeted indentation of 1.2 μm, the RMS relative differences of the entire force-indention curve between the FEM result and the AFM indentation data were 8.43%, 9.72%, 10.12%, 10.53%, and 10.24% at the Poisson's ratio of 0.35, 0.37, 0.39, 0.41, 0.45, respectively, as shown in Fig. 9. The standard deviations of the force at each chosen indentation point during the entire indenting process for the five Poisson's ratios were all less than $4.3E-05$ nN, and the deviation errors with respect to the average simulation results at those indentations were less than 16% (see Fig. 9). According to this sensitivity test result, the Poisson's ratio ranges from 0.35 to 0.45 does not affect the FEM simulation result significantly. Therefore, it is reasonable to choose the Poisson's ratio of the cell as 0.37 in the FEM model.

4. Discussion

The results have demonstrated that the proposed FEM simulation matches the AFM indentation experimental data very well. The proposed FEM takes the heterogeneity, e.g., depth-dependent elasticity, of living cells into account by modeling the cell as a multi-layered elastic-viscoelastic structure. The Young's modulus of different parts of the cell was quantified by dividing the experimental measured force-indentation curve into segments and fitting each part using the corrected Hertz contact model (Faria et al., 2008), which led to more accurate material property estimation for the proposed FEM. Indeed, larger fitting error (16.79%) could be induced when fitting the force-indentation curve as a whole (homogeneous assumption), as shown in Fig. 4. Since under the given experiment condition (slow indenting velocity and large indentation depth), the thin-layer Hertz model is adequate to describe the mechanical behavior of living cells during the slow indentation process (Faria et al., 2008), the above large fitting error is indeed a result of the homogeneous assumption of cells. Therefore, the multi-layer model we proposed is validated. According to Kamm et al. (2000) and Nawaz et al. (2012) (Nawaz et al., 2012; Guilak et al., 2000), the cell nucleus (with a Young's modulus of 400 Pa) is four times harder than the cytoplasm (with a Young's modulus of 100 Pa). In this study, the average Young's modulus of cytoplasm and nucleus quantified were 83 Pa and 390 Pa, respectively, which compared well with the reported values, thus, led to a relatively small difference between the FEM simulation results and experiment data.

As revealed in this study and literature, the cells are depth-dependent in terms of mechanical properties (Faria et al., 2008; Mollaeian et al., 2018). This depth-dependent mechanical behavior of living cells is likely caused by the material heterogeneity, such as the difference of mechanical behavior of the cell components (e.g., membrane, cytoskeleton), and organelle distribution inside the cytoplasm at the different depths. To account for the significant difference of structural components in affecting the cellular mechanical behavior, the living cell in the proposed FEM was divided into three layers. Based on our simulation results, the differences in elastic properties of each component significantly affected the force-indentation relation obtained. During the indenting process, a small jump was always observed when the indentation was around 0.5 μm for each simulation, and it was noticed that the slope of force-indentation changed greatly after this jump, especially for the indentation depth of 1.2 μm. This can be explained by the difference of the material properties between the cytoplasm and nucleus. At the beginning of the indentation process, most of the probe-cell interaction force was created by the cytoplasm, together with the cytoskeleton and the cell membrane, so that the slope of the force-indentation curve was much smaller than the latter part, in which the effect of the nucleus (with a much bigger Young's modulus) became more significant as the increase of the indentation depth. Therefore, the simulation results concurred with the experimental results that the slope of the force-indentation curve (represents the cell stiffness) increased as the indentation increase due to the pronounced effect of the cell nucleus.

It has been observed that a slightly bigger difference existed between the FEM simulation and AFM experiment at the indentation depths of 1 μm and 1.2 μm compared to the 0.7 μm result. This increased measurement difference is because the viscoelastic properties of the cell quantified from the AFM relaxation measurement (with 1μm

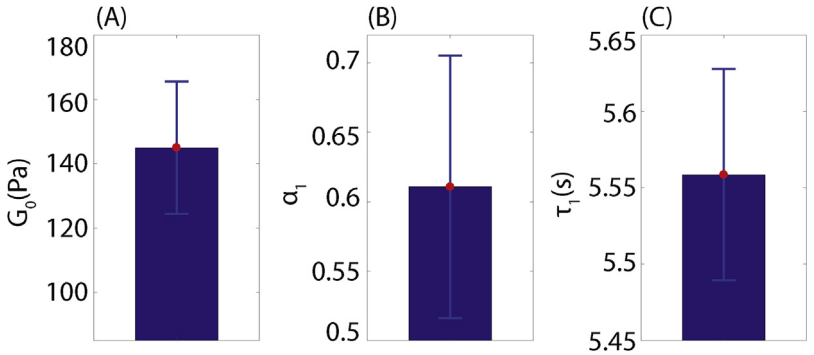

Fig. 7. The quantified viscoelastic parameters: (A) The instantaneous shear modulus $G_0 = 145 \pm 20.555$ Pa, (B) The relative moduli $\alpha_1 = 0.6108 \pm 0.095$. (C) The relaxation time $\tau_1 = 5.56 \pm 0.07$ s. $n = 5$.

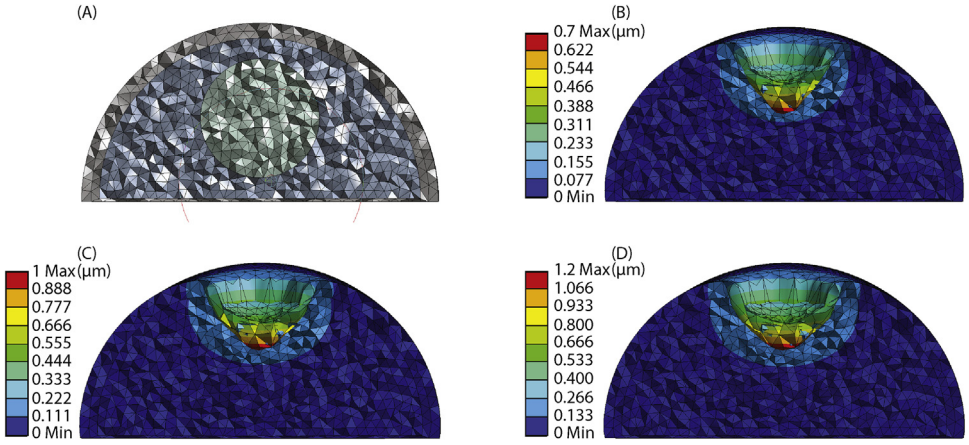

Fig. 8. Cell Deformation (indentation) distribution of the FEM model with the targeted indentation of: (A) 0 μm, (B) 0.7 μm, (C) 1 μm, and (D) 1.2 μm.

initial indentation) were used for all three layers in the FEM model. This approximation didn't affect the 0.7 μm simulation results much as at a small indentation depth (i.e., small intracellular strain) the elastic behavior of the cells was more dominant. However, for the indentation depth of 1 μm and higher, the material heterogeneity in viscoelasticity may need to be considered. This argument can be verified by Fig. 9, where the simulation curves were very close to the AFM experiment data when the indentation was small, and the difference between these two increases gradually with the indentation. However, living cells are complex active materials after all, it is impossible to generate a simulation model to match the real living cells perfectly. The approximated three-layered semi-ellipsoid cell shape, the AFM indentation measurement uncertainties, as well as the measurement condition variation (e.g., temperature, CO_2 level) can all lead to the difference between the simulation results and the experiment data observed in this study. Considering these facts, the less than 10% simulation difference demonstrated that the proposed FEM model is accurate enough to simulate the mechanical behavior of living cells at low indenting velocity and can be used for biomechanical analysis of cell behavior under matching mechanical loading conditions.

We have noticed that the simulation results were very sensitive to the indenting velocity. It is of importance to note that the material property estimation in this study (see Eqs. (3) and (12)) was under the assumption of uniformly distributed intracellular stress (i.e., slow indenting velocity). Therefore, for FEM simulation of cell mechanical behavior under high speed loadings, a different material property estimation approach needs to be established. As shown in previous studies (Moeendarbary et al., 2013; Mollaeian et al., 2018; Ren et al., 2013), living cell mechanical behavior is also loading velocity/frequency dependent due to the viscoelastic nature of the cells, therefore, the viscoelastic heterogeneity cannot longer be ignored under these conditions. Furthermore, it has been shown that poroelastic behavior is dominant during the force relaxation measurements immediately after high-speed indentation (Moeendarbary et al., 2013; Mollaeian et al., 2018), therefore, the proposed FEM can be further improved by including the material poroelastic property, especially for the cytoplasm layer.

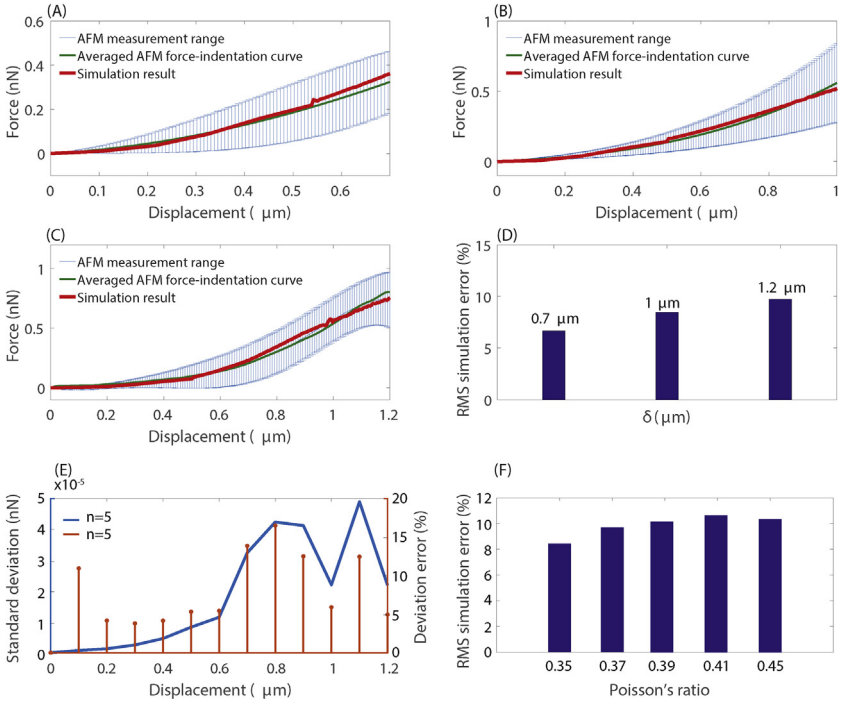

Fig. 9. Comparison of the FEM simulated force-indentation curve with the AFM experiment results at the targeted indentation of (A) 0.7 μm, (B) 1 μm, and (C) 1.2 μm. The blue error bars denote the data range of the AFM experimental results, the green curve is the averaged force-indentation curve of the experimental results. (D) The RMS FEM simulation error with respect to the averaged experiment curve. (E) The standard deviation of the FEM force vs. displacement relation (blue curve) when the cell Poisson's ratio of 0.35, 0.37, 0.39, 0.41, and 0.45. The orange stems are the deviation error with respect to the average simulation results. (F) The RMS FEM simulation error with respect to the AFM measurement curve at the final indentation of 1.2 μm for each tested Poisson's ratio.

5. Conclusion

A new FEM model was proposed in this study to account for the depth-dependent mechanical behavior of living cells. The geometric size of the three-layered FEM cell model was determined by using AFM topography images, and the mechanical properties of the cell layers were quantified using AFM indentation measurement by accounting for both the cellular elasticity and viscoelasticity. The proposed FEM was validated by comparing the simulated force-indentation curves with the experimental AFM data, and the simulation error was less than 10% with respect to the experiment results for all of the tested conditions. Considering the measurement uncertainty, the proposed FEM model was quite accurate in terms of simulating the force response of living NIH/3T3 cells. Therefore, the proposed FEM has a great potential to be implemented for intracellular force transduction and distribution simulation to promote further understandings of mechanotransduction.

Acknowledgments

This work was supported by the National Science Foundation (NSF) [CMMI-1634592], and Iowa State University. The authors also thank Dr. Xuefeng Wang for providing NIH/3T3 cells.

References

Abu-Lail, N.I., Ohashi, T., Clark, R.L., Erickson, H.P., Zauscher, S., 2006. Understanding the elasticity of fibronectin fibrils: unfolding strengths of FN-III and GFP domains measured by single molecule force spectroscopy. Matrix Biol. 25 (3), 175–184.
Amano, M., Ito, M., Kimura, K., Fukata, Y., Chihara, K., Nakano, T., Matsuura, Y., Kaibuchi, K., 1996. Phosphorylation and activation of myosin by rho-associated kinase (rho-kinase). J. Biol. Chem. 271 (34), 20246–20249.
Baaijens, F.P., Trickey, W.R., Laursen, T.A., Guilak, F., 2005. Large deformation finite element analysis of micropipette aspiration to determine the mechanical properties of the chondrocyte. Ann. Biomed. Eng. 33 (4), 494–501.
Bursa, J., Fuis, V., 2009. Finite element simulation of mechanical tests of individual cells. IFMBE Proc. WC 16–19.
Caille, N., Thoumine, O., Tardy, Y., Meister, J.-J., 2002. Contribution of the nucleus to the mechanical properties of endothelial cells. J. Biomech. 35 (2), 177–187.
Chen, J., Lu, G., 2012. Finite element modelling of nanoindentation based methods for mechanical properties of cells. J. Biomech. 45 (16), 2810–2816.
Chen, W., Zhu, C., 2013. Mechanical regulation of T-cell functions. Immunol. Rev. 256 (1), 160–176.
Chen, J., 2014. Nanobiomechanics of living cells: a review. Interface Focus 4 (2), 20130055.
Chung, C.-Y., Mansour, J.M., 2014. Application of Ansys to the stress relaxation of articular cartilage in unconfined compression. J. Chin. Inst. Eng. 37 (3), 376–384.
Clynes, M., 2012. Animal Cell Culture Techniques. Springer Science & Business Media.
Darling, E., Zauscher, S., Guilak, F., 2006. Viscoelastic properties of zonal articular chondrocytes measured by atomic force microscopy. Osteoarthritis Cartilage 14 (6), 571–579.
Del Nobile, M., Chillo, S., Mentana, A., Baiano, A., 2007. Use of the generalized Maxwell model for describing the stress relaxation behavior of solid-like foods. J. Food Eng. 78 (3), 978–983.
Efremov, Y.M., Wang, W.-H., Hardy, S.D., Geahlen, R.L., Raman, A., 2017. Measuring nanoscale viscoelastic parameters of cells directly from AFM force-displacement curves. Sci. Rep. 7 (1), 1541.
Evans, E., Heinrich, V., Leung, A., Kinoshita, K., 2005. Nano-to microscale dynamics of P-selectin detachment from leukocyte interfaces. I. Membrane separation from the cytoskeleton. Biophys. J. 88 (3), 2288–2298.
Faria, E.C., Ma, N., Gazi, E., Gardner, P., Brown, M., Clarke, N.W., Snook, R.D., 2008. Measurement of elastic properties of prostate cancer cells using AFM. Analyst 133 (11), 1498–1500.
Giridharagopal, R., Rayermann, G.E., Shao, G., Moore, D.T., Reid, O.G., Tillack, A.F., Masiello, D.J., Ginger, D.S., 2012. Submicrosecond time resolution atomic force microscopy for probing nanoscale dynamics. Nano Lett. 12 (2), 893–898.
Gosse, C., Croquette, V., 2002. Magnetic tweezers: micromanipulation and force measurement at the molecular level. Biophys. J. 82 (6), 3314–3329.
Guilak, F., Mow, V.C., 2000. The mechanical environment of the chondrocyte: a biphasic finite element model of cell-matrix interactions in articular cartilage. J. Biomech. 33 (12), 1663–1673.
Guilak, F., Tedrow, J.R., Burgkart, R., 2000. Viscoelastic properties of the cell nucleus. Biochem. Biophys. Res. Commun. 269 (3), 781–786.
Honarmandi, P., Lee, H., Lang, M.J., Kamm, R.D., 2011. A microfluidic system with optical laser tweezers to study mechanotransduction and focal adhesion recruitment. Lab Chip 11 (4), 684–694.
Hutter, J.L., Bechhoefer, J., 1993. Calibration of atomic-force microscope tips. Rev. Sci. Instrum. 64 (7), 1868–1873.
Kaliske, M., Rothert, H., 1997. Formulation and implementation of three-dimensional viscoelasticity at small and finite strains. Comput. Mech. 19 (3), 228–239.
Liu, B., Shao, J.-Y., 2014. Micropipette aspiration and subcellular biophysics. Approximate Analytical Methods for Solving Ordinary Differential Equations. pp. 325.
Liu, K.-K., 2006. Deformation behaviour of soft particles: a review. J. Phys. D: Appl. Phys. 39 (11), R189.
Lyon, R.C., Zanella, F., Omens, J.H., Sheikh, F., 2015. Mechanotransduction in cardiac hypertrophy and failure. Circ. Res. 116 (8), 1462–1476.
Mathieu, P., Loboa, E., 2012. Cytoskeletal and focal adhesion influences on mesenchymal stem cell shape, mechanical properties, and differentiation down osteogenic, adipogenic, and chondrogenic pathways. Tissue Eng. Part B: Rev. 18 (6), 436–444.
McGarry, J., Prendergast, P., 2004. A three-dimensional finite element model of an adherent eukaryotic cell. Eur. Cell Mater. 7, 27–33.
Mijailovich, S.M., Kojic, M., Tsuda, A., 2010. Particle-induced indentation of the alveolar epithelium caused by surface tension forces. J. Appl. Physiol. 109 (4), 1179–1194.
Moeendarbary, E., Harris, A.R., 2014. Cell mechanics: principles, practices, and prospects. Wiley Interdiscip. Rev.: Syst. Biol. Med. 6 (5), 371–388.
Moeendarbary, E., Valon, L., Fritzsche, M., Harris, A.R., Moulding, D.A., Thrasher, A.J., Stride, E., Mahadevan, L., Charras, G.T., 2013. The cytoplasm of living cells behaves as a poroelastic material. Nat. Mater. 12 (3), 253.
Mollaeian, K., Liu, Y., Bi, S., Ren, J., 2018. Atomic force microscopy study revealed velocity-dependence and nonlinearity of nanoscale poroelasticity of eukaryotic cells. J. Mech. Behav. Biomed. Mater. 78, 65–73.
Nawaz, S., Sánchez, P., Bodensiek, K., Li, S., Simons, M., Schaap, I.A., 2012. Cell viscoelasticity measured with AFM and optical trapping at sub-micrometer deformations. PLoS ONE 7 (9), e45297.
Paul, J., et al., 1970. Cell and Tissue Culture, 4th ed. .
Polacheck, W.J., German, A.E., Mammoto, A., Ingber, D.E., Kamm, R.D., 2014. Mechanotransduction of fluid stresses governs 3D cell migration. Proc. Natl. Acad. Sci. 111 (7), 2447–2452.
Previtera, M.L., 2014. Mechanotransduction in the immune system. Cell. Mol. Bioeng. 7 (3), 473–481.
Ren, J., Yu, S., Gao, N., Zou, Q., 2013. Indentation quantification for in-liquid nanomechanical measurement of soft material using an atomic force microscope: rate-dependent elastic modulus of live cells. Phys. Rev. E 88 (5), 052711.
Sedef, M., Samur, E., Basdogan, C., 2006. Real-time finite-element simulation of linear viscoelastic tissue behavior based on experimental data. IEEE Comput. Graph. Appl. 26 (6).
Shaw, P., Brown, J., 2012. Nucleoli: composition, function, and dynamics. Plant Physiol. 158 (1), 44–51.
Shin, D., Athanasiou, K., 1999. Cytoindentation for obtaining cell biomechanical properties. J. Orthop. Res. 17 (6), 880–890.
Stansfield, W.E., Ranek, M., Pendse, A., Schisler, J.C., Wang, S., Pulinilkunnil, T., Willis, M.S., 2014. The pathophysiology of cardiac hypertrophy and heart failure. Cellular and Molecular Pathobiology of Cardiovascular Disease. Elsevier, pp. 51–78.
Trickey, W.R., Baaijens, F.P., Laursen, T.A., Alexopoulos, L.G., Guilak, F., 2006. Determination of the Poisson's ratio of the cell: recovery properties of chondrocytes after release from complete micropipette aspiration. J. Biomech. 39 (1), 78–87.
Wozniak, M.A., Chen, C.S., 2009. Mechanotransduction in development: a growing role for contractility. Nat. Rev. Mol. Cell Biol. 10 (1), 34–43.
Yan, B., Wang, X., Shi, P., 2017. Risk assessment and control of agricultural supply chains under internet of things. Agrekon 56 (1), 1–12.
Yeganeh-Haeri, A., Weidner, D.J., Parise, J.B., 1992. Elasticity of α-cristobalite: a silicon dioxide with a negative Poisson's ratio. Science 257 (5070), 650–652.